analytical chemistry

Article

pubs.acs.org/ac

Poly β-Cyclodextrin/TPdye Nanomicelle-based Two-Photon Nanoprobe for Caspase-3 Activation Imaging in Live Cells and Tissues

Huijuan Yan, Leiliang He, Wenjie Zhao, Jishan Li,* Yue Xiao, Ronghua Yang,* and Weihong Tan

State Key Laboratory of Chemo/Biosensing and Chemometrics, College of Chemistry and Chemical Engineering, Hunan University, Changsha 410082, People's Republic of China

Supporting Information

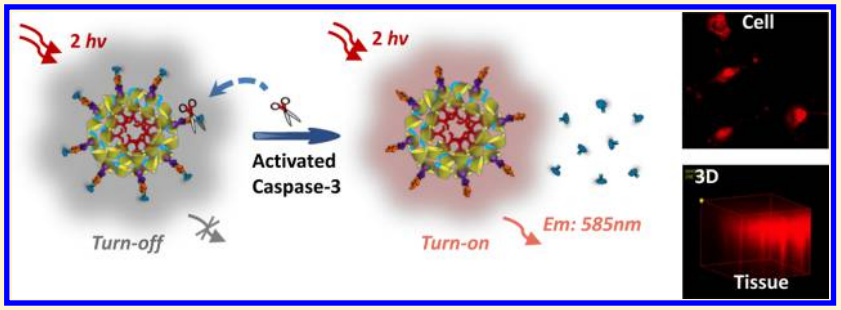

ABSTRACT: Two-photon excitation (TPE) with near-infrared (NIR) photons as the excitation source has important advantages over conventional one-photon excitation (OPE) in the field of biomedical imaging. β-cyclodextrin polymer (βCDP)-based two-photon absorption (TPA) fluorescent nanomicelle exhibits desirable two-photon-sensitized fluorescence properties, high photostability, high cell-permeability and excellent biocompatibility. By combination of the nanostructured two-photon dye (TPdye)/βCDP nanomicelle with the TPE technique, herein we have designed a TPdye/βCDP nanomicelle-based TPA fluorescent nanoconjugate for enzymatic activity assay in biological fluids, live cells and tissues. This sensing system is composed of a *trans*-4-[*p*-(*N*,*N*-diethylamino)styryl]-*N*-methylpyridinium iodide (DEASPI)/βCDP nanomicelle as TPA fluorophore and carrier vehicle for delivery of a specific peptide sequence to live cell through fast endocytosis, and an adamantine (Ad)-GRRRDEVDK-BHQ2 (black hole quencher 2) peptide (denoted as Ad-DEVD-BHQ2) anchored on the DEASPI/βCDP nanomicelle's surface to form TPA DEASPI/βCDP@Ad-DEVD-BHQ2 nanoconjugate by the βCD/Ad host−guest inclusion strategy. Successful in vitro and in vivo enzymatic activities assay of caspase-3 was demonstrated with this sensing strategy. Our results reveal that this DEASPI/βCDP@Ad-DEVD-BHQ2 nanoconjugate not only is a robust, sensitive and selective sensor for quantitative assay of caspase-3 in the complex biological environment but also can be efficiently delivered into live cells as well as tissues and act as a "signal-on" fluorescent biosensor for specific, high-contrast imaging of enzymatic activities. This DEASPI/βCDP@Ad-DEVD-BHQ2 nanoconjugate provides a new opportunity to screen enzyme inhibitors and evaluate the apoptosis-associated disease progression. Moreover, our design also provides a methodology model scheme for development of future TPdye/βCDP nanomicelle-based two-photon fluorescent probes for in vitro or in vivo determination of biological or biologically relevant species.

The progress of fluorescent imaging technology increasingly pushes forward the development of cell biology studies and clinical applications, providing sophisticated understanding to the pathogenesis, progression and treatment of many human diseases.[1] However, the general one-photon excitation (OPE)-based fluorescent imaging strategies have unvanquishable limitations due to the short excitation wavelengths, which would induce large photodamages, high tissue autofluorescence, big photon loss owing to self-absorption and scattering.[2] Thus, two-photon excitation (TPE) with near-infrared (NIR) photons as the excitation source has become more popular in life science and bioimaging applications owing to its excellent advantages, such as lower tissue autofluorescence and self-absorption, reduced photodamage and photobleaching, higher spatial resolution and deeper penetration depth (>500 μm), etc.[3,4]

Of particular importance for TPE approaches is the construction of the two-photon (TP) probes. To date, a variety of TP fluorescent probes have been developed for applications in chemical sensors[5,6] and biological imagings.[7,8] These probes, however, are mainly focused on organic two-photon absorption (TPA) molecules, and are arguably the lack of cell permeability (which requires potentially disruptive loading techniques or high dye concentrations),[9] low

Received: September 22, 2014
Accepted: October 27, 2014
Published: October 27, 2014

absorptivity, poor photobleaching resistance and biocompatibility, as well as weak ability of cellular localization.[10] Moreover, for biomolecules detection, design and synthesis of the organic molecule-based TPA probes are still great challenges. With the rapid advancement of nanotechnology and the desirable properties of nanostructures including antienzyme action,[11] carrier properties,[12−15] a tunable circulation lifetime, enhanced permeability and retention (EPR) effect,[16] the TPA nanoprobes would provide an alternative for the TPE-based imaging protocols. Dismayingly, although some TPA fluorescent nanoprobes, for example, quantum dots,[17,18] gold/silver nanoclusters[19] and carbon nanomaterials,[20,21] have been elegantly developed and used for bioimagings, the low quantum yield and narrow spectral coverage, the possible cytotoxicity and the requirement for further hydrophilic and complex functional modification process, are still the limitations for their wide range of applications in bioimaging.[22,23] Therefore, the development of new TPA nanoprobes with excellent characteristics such as good biocompatibility, high cell permeability and high TPA action cross-section has become increasingly important and urgent.

β-Cyclodextrin (βCD), a well-known and readily available molecular host, has been extensively investigated in host−guest chemistry for construction of versatile supramolecular aggregations.[24] βCD-based polymers (βCDP) have been extensively used for molecular recognition and drug delivery because of their high solubilization ability, low toxicity and their ability to destabilize and permeate biological membranes and for obviating undesirable side effects.[25] Moreover, βCDP are cyclic oligomers of glucose that can form water-soluble inclusion complexes with small molecules and portions of large compounds.[26] Recently, we have developed a facile strategy for preparation of TPA fluorescent nanomicelle through the "host−guest" chemistry.[27] It has been really surprising to us that this βCDP-based TPA fluorescent nanomicelle exhibits desirable two-photon-sensitized fluorescence properties, high photostability, high cell-permeability, high stability and excellent biocompatibility. Moreover, by anchoring the RGD peptide on the nanomicelle's surface via the high binding affinity of labeled adamantine (Ad) with βCD, the targeted TPE imaging has been successfully achieved in cancer cells and tumor tissues. Therefore, knowing the excellent properties of this βCDP-based TPA fluorescent nanomicelle, fabricating the βCDP-based TPA nanoprobes combined with other biological macromolecules and applying in the TPE imaging, will have a fascinating prospect.

Considering the unique properties of nanostructures and the TPE technique, herein, we designed a βCDP/two-photon dye (TPdye) nanomicelle-based TPA sensing nanoconjugate for caspase-3 activation imaging in live cells or deep tissues (Scheme 1). Caspase-3 has been identified as a key effector caspase, and plays a vital role in mediating the initiation and propagation of the apoptotic cascade.[28] Thus, the ability to image its activation noninvasively will provide a window of opportunity to evaluate therapeutics in live animals and a guide to the design of selective inhibitors to treat caspase-mediated diseases. Although plenty of fluorescent probes with high-sensitivity have been proposed for caspase activation imaging,[29−31] these conventional OPE-based fluorescent strategies are not suitable for applications in complicated biological fluids or in vivo imaging, and at the same time the efficient TPA nanoprobes for caspase-3 activation imaging appear to be rare. Thus, we prepared a βCDP/TPdye

Scheme 1. (A) Schematic Illustration of the DEASPI/βCDP@Ad-DEVD-BHQ2 Nanoconjugate for Caspase-3 Activity Assay. (B) Schematic Diagram of the Nanosensing Conjugate for Caspase-3 Activity Monitoring and Imaging in Live Cells[a]

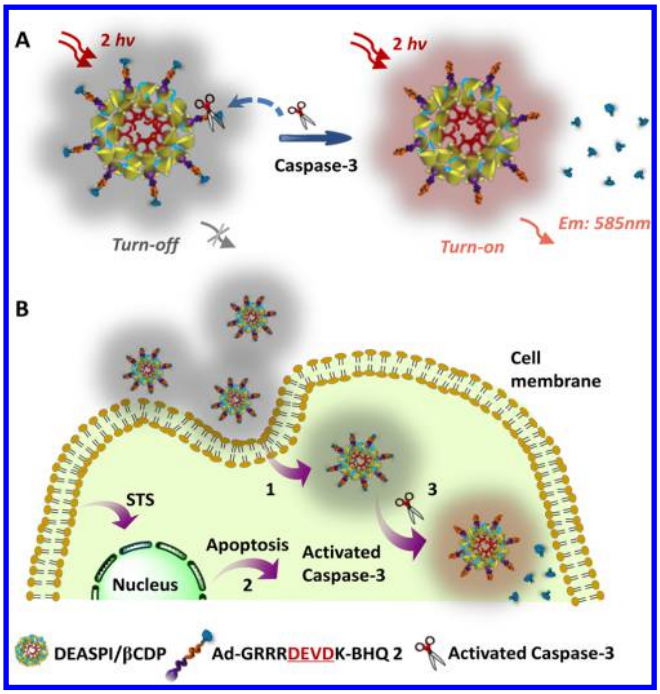

[a](1) Endocytosis; (2) STS (staurosporine, a commonly used apoptosis inducer)-induced cell apoptosis and generate activated caspase-3; (3) cleavage of the DEVD motif and recovery of the TPE fluorescence emission.

nanomicelle-based TPA nanoconjugate as proof-of-concept of the sensing platform for caspase-3 activation assay in complicated biological fluids or live cells as well as deep tissues. The sensing system is composed of a *trans*-4-[*p*-(*N*,*N*-diethylamino)styryl]-*N*-methylpyridinium iodide (DEASPI)/βCDP nanomicelle as TPA fluorophore and carrier vehicles for delivery of a specific peptide sequence to live cell through fast endocytosis, and an Ad-GRRRDEVDK-BHQ2 (black hole quencher 2) peptide (denoted as Ad-DEVD-BHQ2) anchored on the DEASPI/βCDP nanomicelle's surface to form a TPA DEASPI/βCDP@Ad-DEVD-BHQ2 nanoconjugate by the βCD/Ad host−guest inclusion strategy. For the peptide of Ad-GRRRDEVDK-BHQ2, BHQ2 (absorption max at 550 nm) was chosen as an appropriate quencher of the DEASPI via Förster resonance energy transfer (FRET) and GRRRDEVDK was used as a previously described caspase-3 cleavable peptide linker with the cleavage site between D and K. In the apoptosis cells or tumor tissue pretreated with anticancer drug, caspase-3 is processed to its active form,[32] which can cleave the peptide sequence of Ad-GRRRDEVDK-BHQ2 and trigger fluorescence emission recovery of the TPA nanoconjugate.

EXPERIMENTAL SECTION

Chemicals and Instruments. Bovine serum albumin (BSA), human serum albumin (HSA), lysozyme and thrombin were purchased from Sigma-Aldrich. Recombinant human caspase-3 (active form, 10 μg) and a highly specific inhibitor of caspase-3 (Z-DEVD-FMK) were purchased from R&D Systems (Minneapolis, USA). Staurosporine (STS) was

dx.doi.org/10.1021/ac503546r | *Anal. Chem.* 2014, 86, 11440−11450

purchased from Sangon Biotech Co., Ltd. (Shanghai, China). The TPdye (*trans*-4-[*p*-(*N*,*N*-diethylamino)styryl]-*N*-methylpyridinium iodide (DEASPI)) and β-cyclodextrin-based polymers (βCDP) used in this work were synthesized according to our previous report[27] and the molecular structure is shown in Scheme S1 (Supporting Information (SI)). Gly-Arg-Arg-Arg-Asp-Glu-Val-Asp-Lys (GRRRDEVDK) conjugated adamantine and BHQ2 (denoted as Ad-DEVD-BHQ2, purity: 98.5%), GRRRDEVDK conjugated adamantine (denoted as Ad-DEVD, purity: 98.5%) and nonspecific peptide sequence of Gly-Arg-Gly-Asp-Cys conjugated Rhodamine B (denoted as RhB-GRGDC, purity: 98.5%) were purchased from ChinaPeptides Co., Ltd. (Shanghai, China). Methyl thiazolyl tetrazolium (MTT) was purchased from Sigma-Aldrich. 3-[(3-Cholamidopropyl)dimethylammonio]propanesulfonate (CHAPS) and sucrose were purchased from Sun Chemical Technology Co., Ltd. (Shanghai, China). Dithiothreitol (DTT) was purchased from Bio Basic Inc. (Toronto, Canada). 2-[4-(2-Hydroxyethyl)-1-piperazinyl]ethanesulfonic acid (HEPES) and Ethylene Diamine Tetraacetic Acid (EDTA) were purchased from Beijing Dingguo Changsheng Biotechnology Co., Ltd. (Beijing, China). The HeLa (cervical cancer) cell lines and cervical cancer tissue slices obtained from mouse were provided by the Biomedical Engineering Center of Hunan University (China). Other chemicals obtained from commercial suppliers were analytical grade and used without further purification. All solutions were prepared using ultrapure water, which was obtained through a Millipore Milli-Q water purification system (Billerica, MA, USA) and had an electric resistance >18.3 MΩ.

Scanning Electron Microscopy (SEM) (JSM-6700F) and dynamic light scattering (Malvern Zetasizer 3000HS) were employed. High-performance liquid chromatography (HPLC) analysis was performed using a LC-20AT HPLC system (Shimadzu, Japan). UV−vis absorption spectra were measured on a Hitachi U-4100 UV/vis spectrometer (Kyoto, Japan) using a quartz cuvette having 1 cm path length. One-photon excitation (OPE) fluorescence spectra were performed on a PTI ASOC-10 Fluorescence System (Photo Technology International, Birmingham, NJ, USA). Two-photon excitation (TPE) fluorescence spectra were obtained with a mode-locked Ti: sapphire pulsed laser (Chameleon Ultra II, Coherent Inc.) and then recording with a DCS200PC single photon counting (Beijing Zolix Instruments Co., Ltd.). For MTT assay, the spectrophotometrical absorbance of each well was measured by using a Tecan microplate (ELISA) reader (Bio-Rad ELISA reader, Hercules, CA). Two-photon excitation fluorescence images (TPFI) of cells or tissue slices were obtained using an Olympus FV1000-MPE multiphoton laser scanning confocal microscope (Japan). The pH values were calibrated with a model 868 pH meter (Orion).

Preparation of DEASPI/βCDP@Ad-DEVD-BHQ2 Nanoconjugate. For fabrication of the nanoconjugate, the DEASPI/βCDP nanomicelle was first prepared according to our previous report.[27] Briefly, βCDP was suspended in HEPES buffer at a final concentration of 0.75 mg/mL and 0.5 mM DEASPI was added into the above solution at a final concentration of 50 μM. The mixture was stirred for 1 h to form the DEASPI/βCDP nanomicelle. Then, Ad-DEVD-BHQ2 (or Ad-DEVD) was added to the DEASPI/βCDP nanomicelle solution at a final concentration of 0.25 mM and incubated for 4 h at room temperature to guarantee the anchoring of the peptide sequences on the surface of DEASPI/βCDP nanomicelle. Then the mixture was filtrated with an Amicon YM-10 filter to get rid of the free peptide sequences, and the obtained DEASPI/βCDP@Ad-DEVD-BHQ2 (or DEASPI/βCDP@Ad-DEVD) nanoconjugate (concentration of the nanoconjugate refers to the concentration of βCDP, ∼0.75 mg/mL) was resuspended in HEPES buffer and stored at 4 °C before use.

HPLC Analysis. For HPLC analysis of the caspase-3 activity, the sample was prepared as the following description: an aliquot of 5 μL of 500 μM Ad-DEVD-BHQ2 (or RhB-GRGDC, or K-BHQ2) in aqueous solution was added to 90 μL of reaction buffer (pH 7.4, 50 mM HEPES, 10 mM DTT, 100 mM NaCl, 1 mM EDTA, 0.1% w/v CHAPS, 10% sucrose) with/without a highly specific caspase-3 inhibitor Z-DEVD-FMK (the final concentration is 100 μM), then 5 μL of caspase-3 (final concentration is 15 nM) or other DEVD-nonspecific proteins/enzymes with the final concentration of 1.5 μM including bovine serum albumin (BSA), human serum albumin (HSA), thrombin or lysozyme was added and the solution was incubated at 37 °C for 60 min. After reaction, an aliquot of each resulting solution (10 μL) was loaded onto a C18 column (Shimadzu, Japan) fitted on an LC-20AT HPLC system, and the eluate was monitored with a photodiode array detector. Detection wavelength was kept at the maximum absorption wavelength of BHQ2 (λ_{max} = 550 nm) or Rh B (λ_{max} = 540 nm), and the flow rate was set at 1.0 mL/min. Milli-Q water containing 0.1% TFA (A) and MeCN (B) was used as developing solvents.

In Vitro Assay of Caspase-3 Activity Using DEASPI/βCDP@Ad-DEVD-BHQ2 Nanoconjugate. In a typical caspase-3 activity assay using the DEASPI/βCDP@Ad-DEVD-BHQ2 nanoconjugate, an aliquot of 3 μL of the prepared DEASPI/βCDP@Ad-DEVD-BHQ2 conjugate suspension was added to 292 μL of reaction buffer (pH 7.4, 50 mM HEPES, 10 mM DTT, 100 mM NaCl, 1 mM EDTA, 0.1% w/v CHAPS, 10% sucrose) or cell media (RPMI 1640 supplemented with 10% fetal bovine serum (FBS)), then 5 μL of caspase-3 (final concentrations ranging from 0 to 2.64 nM) or other proteins was added and the solution was incubated at 37 °C for 60 min. After reaction, the resulting solution was subjected to fluorescence measurements. For the OPE measurement, the fluorescence spectra were recorded in a quartz cuvette on PTI QM4 fluorescence system with the excitation wavelength of 470 nm and the emission wavelengths in the range from 500 to 720 nm with both excitation and emission slits of 2.5 nm. The time-dependent OPE fluorescence responses were recoded immediately after the addition of capspase-3 or other proteins at an excitation wavelength of 470 nm (slit 2.5 nm) and an emission wavelength of 585 nm (slit 2.5 nm) with a certain time interval. For the TPE measurement, the two-photon emission fluorescence spectra in the range from 500 to 660 nm were obtained by exciting all samples at 840 nm with a mode-locked Ti:sapphire pulsed laser (Output laser pulses were centered at 840 nm and an average power of 100 mW was as the excitation source. The laser pulses have pulse duration of 120 fs and repetition rate of 80 MHz.), followed by recording with a DCS200PC single photon counting.

Cell Culture, Cellular uptake and Cytotoxicity Assay. For the cellular uptake, HeLa cells were seeded on glass-bottom dishes (Mattek), and were grown until 70−80% confluent. After that, the cells were incubated with 2-deoxyglucose/sodium azide (50 mM/30 mM 2DG/NaN_3, inhibitors of cellular energy metabolism), chlorpromazine (10 μg/mL CPZ, clathrin inhibitor), sucrose (0.45 M, disrupt clathrin-mediated

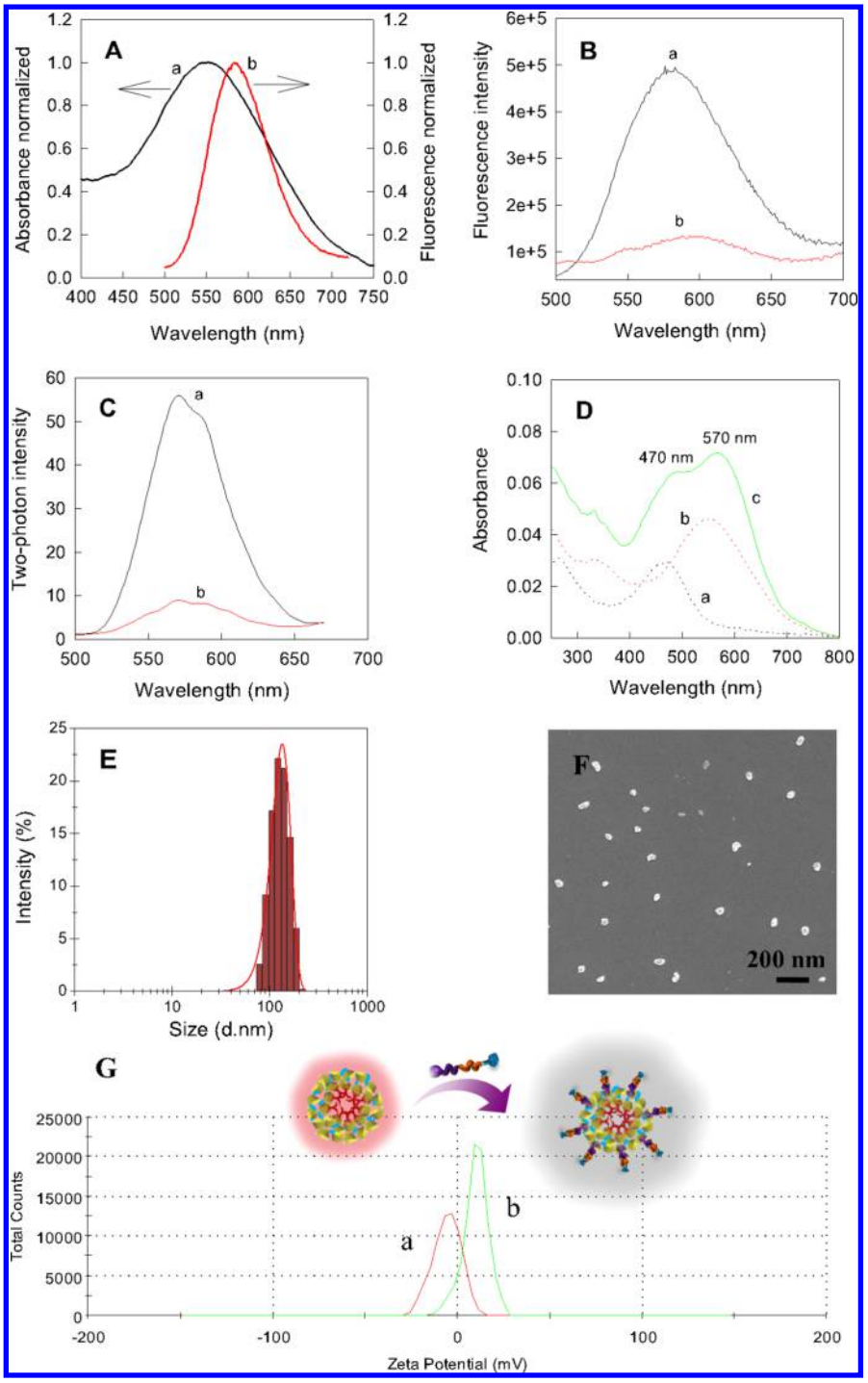

Figure 1. (A) Normalized absorbance spectrum of Ad-DEVD-BHQ2 (curve a) and the normalized emission spectrum of the DEASPI/βCDP nanomicelle (curve b) in HEPES buffer (pH = 7.4). (B) OPE and (C) TPE fluorescence emission spectra of the nanoconjugate aqueous solutions. For "B": a, 500 nM of DEASPI + 7.5 μg/mL of βCDP; b, 500 nM of DEASPI + 7.5 μg/mL of βCDP + 2.5 μM of Ad-DEVD-BHQ2; λ_{ex} = 470 nm. For "C": 10 μM of DEASPI + 0.15 mg/mL of βCDP; b, 10 μM of DEASPI + 0.15 mg/mL of βCDP + 50 μM Ad-DEVD-BHQ2; λ_{ex} = 840 nm. (D) UV−vis absorption spectra of the aqueous solutions of DEASPI/βCDP nanomicelle (curve a), Ad-DEVD-BHQ2 (curve b) and DEASPI/βCDP@Ad-DEVD-BHQ2 nanoconjugate (curve c). (E) DLS data and (F) SEM image of the DEASPI/βCDP@Ad-DEVD-BHQ2 nanoconjugate. (G) The ζ-potentials of DEASPI/βCDP nanomicelle (curve a, −3.76 mV) and DEASPI/βCDP@Ad-DEVD-BHQ2 nanoconjugate (curve b, +10.6 mV).

endocytosis), Filipin (10 μg/mL, caveolae inhibitor), or cytochalasin D (2 μM CD, actin inhibitor) for 1 h at 37 °C. The cells were then washed with culture medium and incubated with DEASPI/βCDP@Ad-DEVD nanoconjugate for 1 h, and finally rinsed with phosphate buffered saline (PBS) (137 mM NaCl, 2.7 mM KCl, 10 mM Na2HPO4, 1.8 mM KH2PO4, pH 7.4). The obtained cells were observed under an Olympus FV1000-MPE multiphoton laser scanning confocal microscope.

For cytotoxicity assay, HeLa cells were cultured in RPMI 1640 supplemented with 10% FBS (Thermo Scientific HyClone). When in the proliferative period, HeLa cells were dispersed within replicate 96-well microliter plates to a total

dx.doi.org/10.1021/ac503546r | Anal. Chem. 2014, 86, 11440−11450

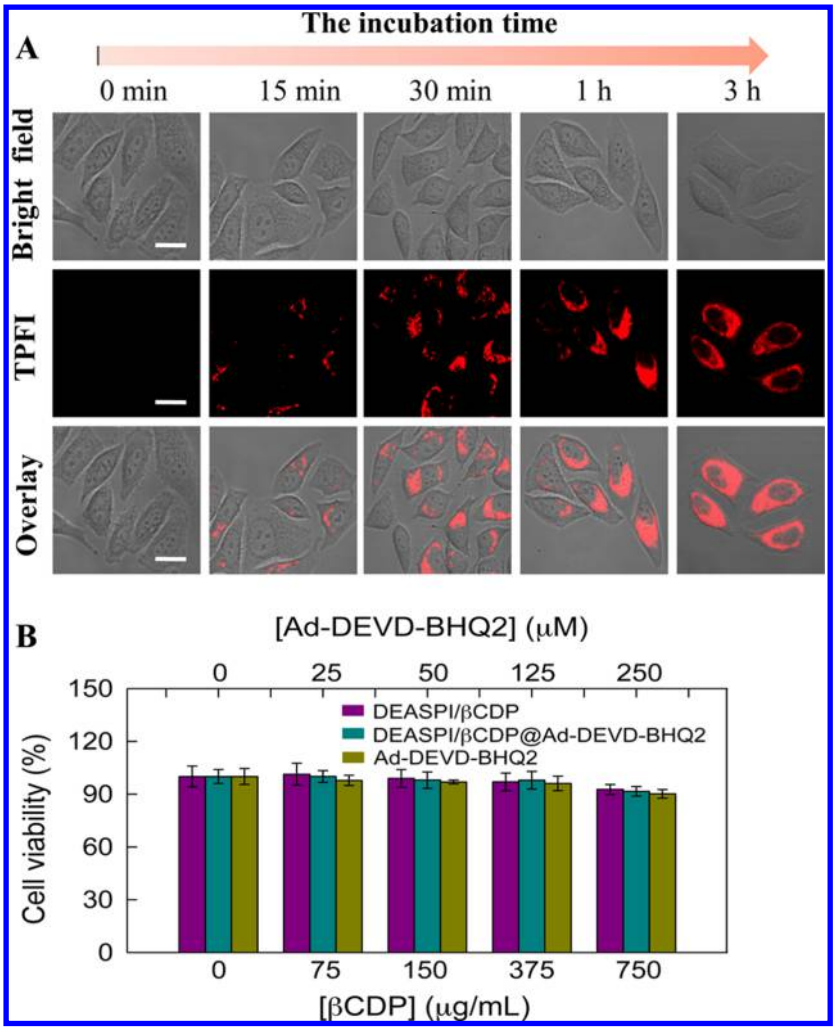

Figure 2. (A) Cellular uptake of the nanoconjugate as a function of incubation time. Experimental steps: 500 μL of fresh cell growth medium supplemented with the prepared DEASPI/βCDP@Ad-DEVD nanoconjugate (0.15 mg/mL, concentration of the nanoconjugate refers to the concentration of βCDP) was added in each well with HeLa cells. After incubation for different times at 37 °C, the treated cells were washed three times with PBS and two-photon confocal fluorescence imaging of the cells was observed under an Olympus FV1000-MPE multiphoton laser scanning confocal microscope, with a mode-locked titanium−sapphire laser source set at wavelength 840 nm. Scale bars: 20 μm. (B) Cell viability values (%) estimated by MTT proliferation. HeLa cells were incubated with 0−0.75 mg/mL DEASPI/βCDP@Ad-DEVD-BHQ2 nanoconjugate (DK Cyan) and DEASPI/βCDP nanomicelle (DK Pink), 0−250 μM Ad-DEVD-BHQ2 (DK Yellow) at 37 °C for 48 h. Cells without added anything were taken as the control experiment, and the viability was set as 100%. The final reported data were expressed as a percentage of the control (mean standard deviation). Three independent experiments containing duplicates were performed.

volume of 100 μL/each well and maintained at 37 °C in a 5% CO_2/95% air incubator for 24 h. Then, the culture media was removed and the cells were incubated in culture medium containing the as-prepared DEASPI/βCDP@Ad-DEVD-BHQ2 nanoconjugate, DEASPI/βCDP nanomicelle, and Ad-DEVD-BHQ2 with different concentrations for 48 h and then washed with the culture medium. An amount of 100 μL of the fresh culture medium containing MTT (0.5 mg/mL) was then added, followed by incubating for 4 h to allow the formation of formazan dye. After the medium was removed, 150 μL of DMSO was added to each well to dissolve the formazan crystals. Absorbance was measured at 490 nm in a Bio-Rad ELISA microplate reader. Relative cell viability was expressed as ([OD]test/[OD]control) × 100%. Each experiment was repeated at least three times.

Live Cell Imaging of Caspase-3 Activity Using DEASPI/βCDP@Ad-DEVD-BHQ2 Nanoconjugate. HeLa cells were seeded on glass-bottom dishes (Mattek) and were grown until 70−80% confluent. Then the growth medium was removed and washed three times with PBS. Then, 500 μL of fresh cell growth medium supplemented with DEASPI/βCDP@Ad-DEVD-BHQ2 nanoconjugate (~0.15 mg/mL, concentration of the nanoconjugate refers to the concentration of βCDP) was added in each well. After incubation for 1 h at 37 °C, the medium was replaced with fresh medium containing staurosporine (STS) of a final concentration of 4 μM, and the cells were incubated for an additional 3.0 h at 37 °C (For the caspase-3 inhibitor assay, cells were coincubated with 100 μM Z-DEVD-FMK according to the manufacturer's protocol.). Finally, the treated cells were washed three times with PBS and two-photon confocal fluorescence imaging of the cells was observed under an Olympus FV1000-MPE multiphoton laser scanning confocal microscope, with a mode-locked titanium-sapphire laser source set at wavelength 840 nm.

Deep Tissue Imaging of Caspase-3 Activity Using DEASPI/βCDP@Ad-DEVD-BHQ2 Nanoconjugate. 1.0 mm

dx.doi.org/10.1021/ac503546r | Anal. Chem. 2014, 86, 11440−11450

thick cervical tumor tissue slices were obtained from the mouse that was pretreated with/without doxorubicin (10 mg/kg) for 24 h. Then the slices were incubated with 0.15 mg/mL DEASPI/βCDP@Ad-DEVD-BHQ2 nanoconjugate (concentration of the nanoconjugate refers to the concentration of βCDP) in 10% bovine serum-containing PBS for 1 h at 37 °C. After the samples were washed with PBS to remove the remaining nanoconjugates, two-photon confocal fluorescence imaging, *Z*-scan imaging and the 3D two-photon confocal fluorescence images collected along the *Z*-direction at depth of 0−360 μm (60× magnification) of this treated tumor tissue slices were observed under an Olympus FV1000-MPE multiphoton laser scanning confocal microscope, with a mode-locked titanium-sapphire laser source set at wavelength 840 nm.

RESULTS AND DISCUSSION

Preparation and Characterization of the DEASPI/βCDP@Ad-DEVD-BHQ2 Nanoconjugate. Combining the excellent optical and biocompatible properties of the βCDP-based TPA fluorescent nanomicelle (DEASPI/βCDP nanomicelle)[27] and the perfect spectra overlap between the absorption band of BHQ2 and the fluorescence emission spectrum of the DEASPI/βCDP nanomicelle (Figure 1A), the novel TPA fluorescent sensing platform for caspase-3 activation assay was fabricated by using TPA DEASPI/βCDP nanomicelle as the donor and BHQ2 as the acceptor through the "'host−guest"' chemistry. One can see from Figure 1B,C that the OPE and TPE fluorescence emission of the DEASPI/βCDP nanomicelle decreased significantly upon addition of Ad-DEVD-BHQ2 and a maximum quenching efficiency of ca. 78% can be reached when the concentration of DEASPI/βCDP nanomicelle was fixed at 500 nM of DEASPI and 7.5 μg/mL of βCDP, respectively (Figure S1 in the Supporting Information), thus indicating energy transfer from the fluorescence emission of DEASPI/βCDP nanomicelle to Ad-DEVD-BHQ2. On the contrary, significantly change of fluorescence emission cannot be observed (only 14%) in the case of incubating DEASPI/βCDP nanomicelle with the same concentration of original BHQ2 without Ad (Figure S2 in the Supporting Information). The effective energy transfer implies that the resulting assembly brings the Ad-DEVD-BHQ2 (energy acceptor) and the DEASPI/βCDP nanomicelle (energy donor) into close proximity via host−guest interaction. At the same time, UV−vis absorption spectrum of the prepared DEASPI/βCDP@Ad-DEVD-BHQ2 nanoconjugate also showed that the nanoconjugate was successfully formed, due to except for the absorption peak corresponding to the DEASPI at 470 nm, a new absorption peak at around 570 nm assigned to BHQ2 appeared (Figure 1D). These facts demonstrate the availability of the presented free hydrophobic cavities of βCD on the DEASPI/βCDP nanomicelle surface and the capacity of this TPA nanomicelle to conjugate with other sensing elements.

Morphology and structure of the DEASPI/βCDP@Ad-DEVD-BHQ2 nanoconjugate were then investigated by using dynamic light-scattering (DLS) and scanning electron microscopy imaging (SEM). DLS showed that the nanoconjugate size produced by DEASPI/βCDP nanomicelle and Ad-DEVD-BHQ2 was about 112.4 nm (Figure 1E), slightly larger than that of the DEASPI/βCDP nanomicelle (∼95.7 nm) (Figure S3A, Supporting Information). Relative to the DLS results, SEM images showed that the morphology of the DEASPI/βCDP@Ad-DEVD-BHQ2 nanoconjugate was also spherical shape (Figure 1F), similar to that of the DEASPI/βCDP nanomicelle (Figure S3B, Supporting Information). These results indicate that the structure and morphology of the nanoconjugate were not changed obviously during the functional modification process. To obtain the surface charge information on the DEASPI/βCDP@Ad-DEVD-BHQ2 nanoconjugate, ζ-potential measurement was also carried out. ζ-Potential of the DEASPI/βCDP@Ad-DEVD-BHQ2 nanoconjugate was determined to be about +10.6 mV, significantly positive shift compared with that of the DEASPI/βCDP nanomicelle (−3.76 mV) because Ad-DEVD-BHQ2 has a PI of 10.1 and is positively charged in neutral solution (Figure 1G). These results also further indicate that the conjugation between activatable caspase-specific peptide and DEASPI/βCDP nanomicelle and the successful formation of the DEASPI/βCDP@Ad-DEVD-BHQ2 conjugate are clearly achieved during self-assembly process.

Cell Penetrability and Cytotoxicity of the Nanoconjugate. For practical cell imaging applications, a nanostructured probe should have good cell membrane penetrability, and at the same time, should not interfere with the metabolism of the living system. So, the cell penetrability of the nanoconjugate (DEASPI/βCDP@Ad-DEVD) toward HeLa cells as the model was first investigated. It can be seen clearly from Figure 2A that this nanoconjugate can enter into cell efficiently after only 30 min of incubation because there is intense fluorescence signal observed, whereas a 4 h or even longer incubation time is needed for the most reported nanoparticle-based fluorescent nontargeted probes enter into cells.[30a,33] These data indicate that the DEASPI/βCDP nanomicelle-based nanoconjugate has the rapid cell membrane penetration capacity. The excellent cell penetrability of this nanoconjugate may be resulted from its strong positive charge surface (Figure S4, Supporting Information) to bind to negatively charged groups on the cell surface and translocate across the plasma membrane,[34] and the desirable ability of βCDP to destabilize and permeate biological membranes and for obviating undesirable side effects.[25] To further elucidate the mechanism of cellular delivery of DEASPI/βCDP@Ad-DEVD nanoconjugate, we studied the effect of low temperature and inhibitors of various endocytotic mechanisms, including 2-deoxyglucose/sodium azide (2DG/NaN_3, inhibitors of cellular energy metabolism), chlorpromazine (CPZ, clathrin inhibitor), sucrose (disrupt clathrin-mediated endocytosis), Filipin (caveolae inhibitor) and cytochalasin D (CD, actin inhibitor) (Figure S5, Supporting Information). As seen in Figure S5H (Supporting Information), a significant difference was observed for the cells with (c: 74.71%) and without (a: the inhibition rate was defined as 0%) 2DG/NaN_3 treatment and at low temperature (4 °C, b: 78.31%), thus indicating that the cell entry of the nanoconjugate is an energy and temperature-dependent endocytosis.[35,36] Furthermore, CPZ or sucrose can significantly inhibit the uptake of HeLa cells and the inhibition rate was 73.59% (d) or 78.98% (e), respectively. But Filipin and CD had no significant effect on cell uptake (f, 11.01%; g, 10.56%). All together, the inhibitor experiments suggest that the intracellular internalization of the nanoconjugate is mainly through a clathrin-mediated mechanism. Then cytotoxicity of the DEASPI/βCDP@Ad-DEVD-BHQ2 conjugate toward HeLa cells as the model was also evaluated using the standard cell viability assay, the MTT (3-(4,5-dimethylthiazol-2-yl)-2,5-diphenyltetrazolium bromide) assay.[37] Here we compared the biological toxicity of the DEASPI/βCDP@Ad-DEVD-BHQ2

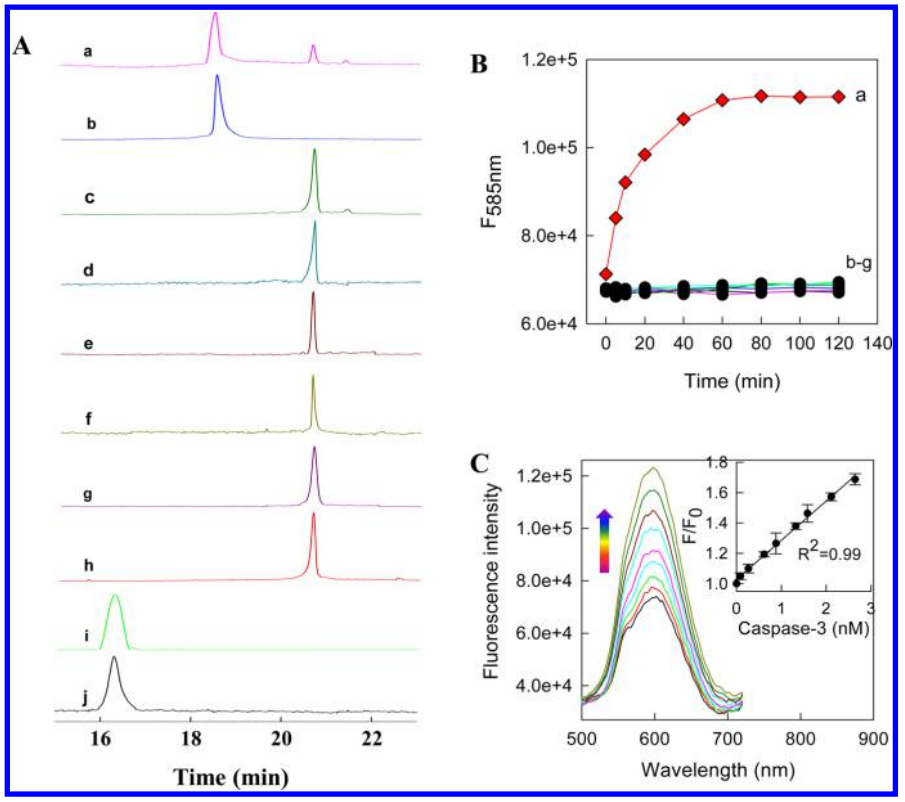

Figure 3. (A) HPLC analysis of the caspase-3 activity. Curve a, Ad-DEVD-BHQ2 (25 μM) + caspase-3 (15 nM); curve b, K-BHQ2 (25 μM); curve c, Ad-DEVD-BHQ2 (25 μM); curve d, Ad-DEVD-BHQ2 (25 μM) + Z-DEVD-FMK (100 μM) + caspase-3 (15 nM); curves e–h, Ad-DEVD-BHQ2 (25 μM) + BSA (1.5 μM), HSA (1.5 μM), thrombin (1.5 μM) and lysozyme (1.5 μM), respectively; curve i, RhB-GRGDC (25 μM); curve j, RhB-GRGDC (25 μM) + caspase-3 (15 nM). Detection wavelength of λ_{ex} = 550 nm for curves a–h and λ_{ex} = 540 nm for curves i and j was used. (B) Time-dependent OPE fluorescence response of the DEASPI/βCDP@Ad-DEVD-BHQ2 nanoconjugate after the addition of capspase-3 or other proteins at an excitation wavelength of 470 nm (slit 2.5 nm) and an emission wavelength of 585 nm (slit 2.5 nm) with a certain time interval (the concentration of the nanoconjugate refers to the concentration of βCDP, ca. 7.5 μg/mL). Curve a, + caspase-3 (1.5 nM); curve b, without caspase-3 as the control; curve c, + Z-DEVD-FMK (10 μM) + caspase-3 (1.5 nM); curve d, + BSA (0.15 μM); curve e:, + HSA (0.15 μM); curve f, + thrombin (0.15 μM); curve g, + lysozyme (0.15 μM). (C) Fluorescence emission spectra of DEASPI/βCDP@Ad-DEVD-BHQ2 nanoconjugate (7.5 μg/mL, concentration of the nanoconjugate refers to the concentration of βCDP) upon various concentrations of caspase-3 (from bottom to up: 0, 0.08, 0.26, 0.62, 0.88, 1.32, 1.58, 2.11 and 2.64 nM, respectively). Inset: linear plot of the relative fluorescence emission intensity (F/F_0) at 585 nm of the DEASPI/βCDP@Ad-DEVD-BHQ2 nanoconjugate versus the concentration of caspase-3. F and F_0 represent the fluorescence emission intensity of the reaction solution in the presence and absence of caspase-3, respectively. Data were presented as average ± SD from three independent measurements. The experimental steps are described in the Experimental Section.

nanoconjugate with the DEASPI/βCDP nanomicelle. After being cultured by the two nanostructures for 48 h, the cellular viability displays that both the DEASPI/βCDP@Ad-DEVD-BHQ2 nanoconjugate and the DEASPI/βCDP nanomicelle possess excellent cell viability. And no significant difference in the proliferation of the HeLa cells is observed in the absence or presence of the two nanostructures even when their concentrations are increased up to 0.75 mg/mL (concentration of the nanostructure refers to the concentration of βCDP) (Figure 2B). The MTT results show that the DEASPI/βCDP@Ad-DEVD-BHQ2 nanoconjugate has no obvious cytotoxic effect on the living system. The high biocompatibility of βCDP may be the cause of the considerably low cytotoxicity of these nanoconjugates to cells. The good cell membrane penetrability and the high biocompatibility of the DEASPI/βCDP@Ad-DEVD-BHQ2 nanoconjugate make it indicate great prospect for cell imaging applications.

Validation of the Sensing Scheme. Scheme 1 illustrates the signaling mechanism of the DEASPI/βCDP@Ad-DEVD-BHQ2 nanosensing conjugate. Before sensing exploration of the nanosensing conjugate, cleavage ability of the caspase-3 to its substrate of DEVD-contained peptide sequence (Ad-DEVD-BHQ2) was first investigated carefully by using HPLC. One can see from Figure 3A that a new obvious peak at about 18.45 min, which is identical to the retention time of K-BHQ2, was observed besides the decreased peak at 20.63 min of the Ad-DEVD-BHQ2 in the presence of caspase-3 (curve a). In contrast, only one peak attributed to the original substrate can be observed for those incubated mixtures, for example, the mixture of Ad-DEVD-BHQ2, the recombinant human caspase-3 and a highly specific caspase-3 inhibitor Z-DEVD-FMK (curve d),[30a,38] the mixture of Ad-DEVD-BHQ2 and other DEVD-nonspecific proteins/enzymes including bovine serum albumin (BSA), human serum albumin (HSA), thrombin or lysozyme (curves e–h), as well as the mixture of a nonspecific peptide sequence of RhB-GRGDC and the recombinant human caspase-3 (curve j), indicating that the caspase-3 has high cleavage efficiency, selectivity and specificity to its substrate of DEVD-contained peptide sequence, thus guaranteeing the desirable performance of the protease sensor for caspase-3 detection.

To verify this design scheme, we then investigate the real-time records of OPE fluorescence intensity changes of the DEASPI/βCDP@Ad-DEVD-BHQ2 nanosensing conjugate in

dx.doi.org/10.1021/ac503546r | Anal. Chem. 2014, 86, 11440–11450

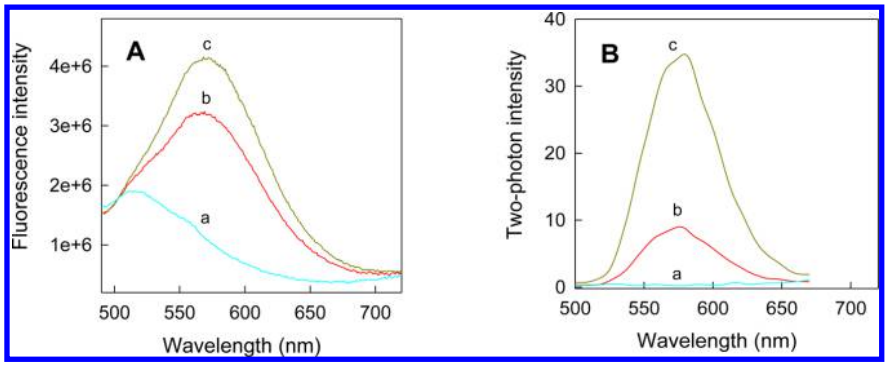

Figure 4. (A) OPE and (B) TPE fluorescence emission spectra of the DEASPI/βCDP@Ad-DEVD-BHQ2 nanoconjugate (0.15 mg/mL, concentration of the nanoconjugate refers to the concentration of βCDP) under the absence (curve b) or presence (curve c, the final concentration of caspase-3 is 30 nM) of caspase-3 in cell growth medium. Cell growth medium without the nanoconjugate and caspase-3 was taken as the control experiment (curve a). The experimental steps are described in the Experimental Section.

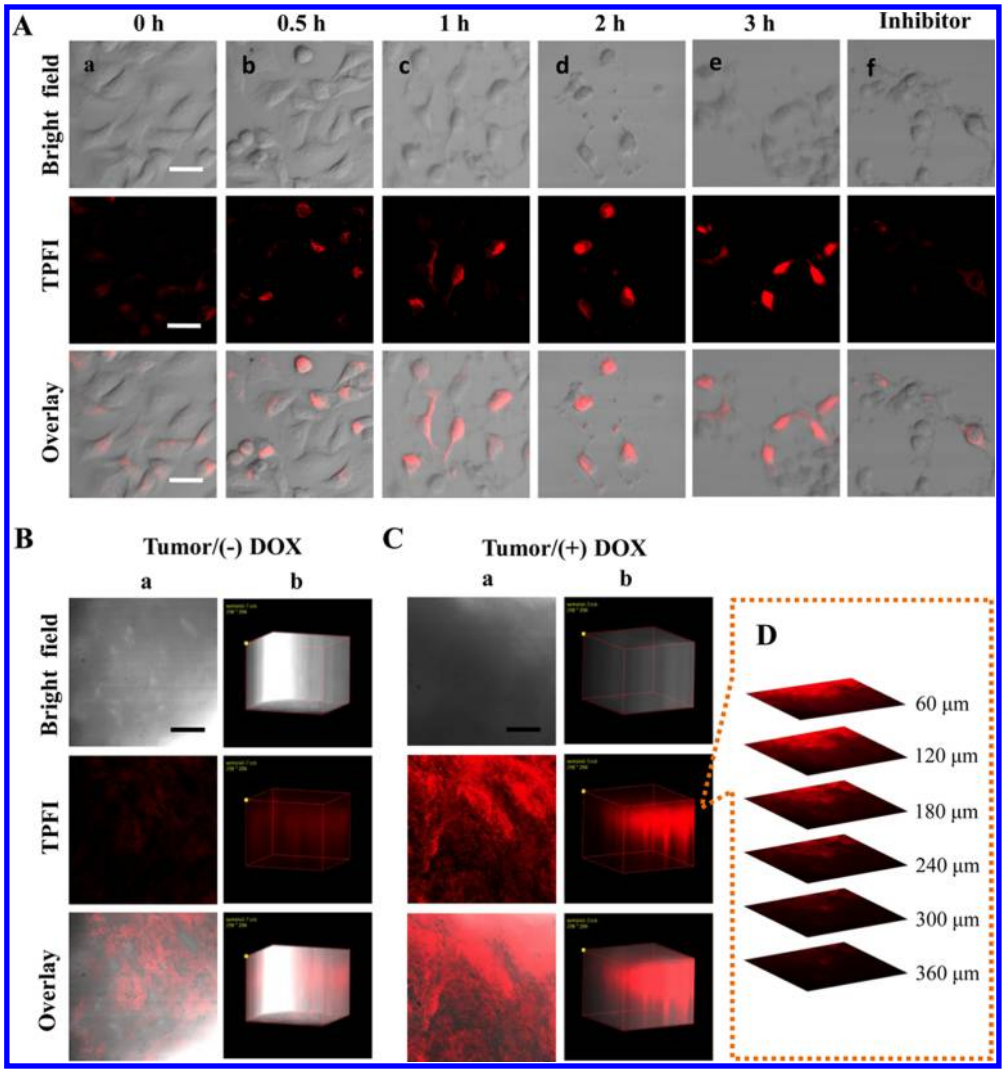

Figure 5. (A) TPM images of HeLa cells treated with 4 μM STS for 0 h (a), 0.5 h (b), 1 h (c), 2 h (d) and 3 h (e), respectively, after incubating with DEASPI/βCDP@Ad-DEVD-BHQ2 nanoconjugate; (f) TPM image of HeLa cells treated with 4 μM STS and 100 μM caspase-3 inhibitor Z-DEVD-FMK for 3 h and then incubated with the nanoconjugate for 1 h at 37 °C. TPM images of the 1.0 mm thick cervical tumor tissue slice pretreated with (C) or without (B) doxorubicin after incubating with DEASPI/βCDP@Ad-DEVD-BHQ2 nanoconjugate (0.15 mg/mL, concentration of the nanoconjugate refers to the concentration of βCDP); (a) the TPE images at a depth of 120 μm and (b) the corresponding 3D images accumulated along the Z-direction at depth of 60−360 μm; (up) bright-field images, (middle) two-photon fluorescence images (TPFI), and (down) overlay of fluorescence and bright-field images. (D) Confocal Z-scan TPFI sections of the nanoconjugate-incubated apoptotic tumor tissue slice at different penetration depths. For panel A, scale bars: 30 μm. For panels B and C, scale bars: 200 μm.

dx.doi.org/10.1021/ac503546r | *Anal. Chem.* 2014, 86, 11440−11450

buffer solution upon addition of the recombinant human caspase-3 and other enzyme or proteins (Figure 3B). In aqueous buffer solution, the fluorescence emission of the nanosensing conjugate was very weak, indicating the interaction of BHQ2-acceptor with the DEASPI/βCDP nanomicelle-donor, allowing the energy transfer process to occur. Distinct increase of fluorescence emission after recombinant human caspase-3 addition verified the feasibility of the sensing scheme (curve a). On the contrary, there no obviously fluorescence emission intensity changes can be observed if the caspase-3 inhibitor (Z-DEVD-FMK) and other enzyme or proteins including BSA, HSA, thrombin and lysozyme was added, indicating that the cleavage reaction for the DEVD-contained peptide sequence was not occurred (curve b−f). Furthermore, TEM, DLS and ζ-potential of the nanoconjugate after cleavage reaction by using caspase-3 show that the cleavaged product is still spherical shape with an average diameter of 101.5 nm and the surface charge changed to +1.18 mV (Figure S6, Supporting Information). These results agreed well with the above HPLC experiments, suggesting that this DEASPI/βCDP@Ad-DEVD-BHQ2 nanoconjugate could act as a sensor for caspase-3 with desirable "signal-on" architecture. It is worth noting that the fluorescence intensity changes of the DEASPI/βCDP@Ad-DEVD-BHQ2 nanoconjugate reached equilibrium within 60 min. Accordingly, 60 min was adopted as the incubation time for the next sensing experiments.

We then investigated the capabilities of the DEASPI/βCDP@Ad-DEVD-BHQ2 nanoconjugate as a protease sensor for in vitro assay of caspase-3 activity. Mixtures of DEASPI/βCDP@Ad-DEVD-BHQ2 conjugate and protease were prepared and incubated at 37 °C. The OPE fluorescence spectra were measured in the range from 500 to 720 nm after 60 min of incubation (Figure 3C). One can see from Figure 3C that the fluorescence intensity dynamically increased with increasing caspase-3 concentration and a plot of fluorescence at the maximum emission wavelength of 585 nm versus caspase-3 concentration in the range from 0.09 to 2.64 nM revealed a linear response characteristic ($R^2 = 0.99$) of the protease sensor, with a readily achieved detection limit of 20 pM.

DEASPI/βCDP@Ad-DEVD-BHQ2 Nanoconjugate for Caspase-3 Activation Measurement in Biological Fluids by OPE and TPE Techniques. Measurement in complex biological samples often suffers from the high fluorescence background produced by the ubiquitous endogenous components in the sample matrix, failing the commonly used biosensors without sample pretreatment.[39] The TPE-based fluorescence strategy with NIR photons as the excitation source might be one of the best choices for the complex biological sample assay. To evaluate the performance of the DEASPI/βCDP@Ad-DEVD-BHQ2 nanoconjugate in complex conditions, we carried out the fluorescence measurements of this nanosensing conjugate in RPMI 1640 cell media upon addition of the recombinant human caspase-3 using OPE and TPE techniques (Figure 4). One can see from Figure 4A that the cell growth media had a high autofluorescence and dominated the fluorescence spectra from 500 to 600 nm under the OPE. Furthermore, the background fluorescence emission was very strong when the target caspase-3 is not presented and significant fluorescence emission increase cannot be obtained even if the recombinant human caspase-3 was added, thus failing to measure the target successfully. However, Figure 4B showed that the TPE fluorescence emission was weak when the target caspase-3 was not presented, whereas remarkable enhancement was observed in the presence of the recombinant human caspase-3. These results suggest that this DEASPI/βCDP@Ad-DEVD-BHQ2 conjugate is a promising fluorescence nanosensor for TPE imaging applications in complex biological samples and the TPE method is more suitable for biological assays compared with the OPE-based methods, owing to the low background fluorescence.

DEASPI/βCDP@Ad-DEVD-BHQ2 Nanoconjugate for Caspase-3 Activation Imaging in Live Cells and Tissues by TPM. After interrogating the response characteristics of the TP protease sensor in vitro, we then explored its potential for live-cell imaging of caspase-3 activation. Human cervix carcinoma (HeLa) cells were first incubated with DEASPI/βCDP@Ad-DEVD-BHQ2 nanoconjugate in the cell growth medium for 1 h at 37 °C. Then, the cells were treated with staurosporine (STS, 4 μM), a commonly used apoptosis inducer,[31b,40] for another different time, and finally the fluorescence emission images were obtained with two-photon confocal microscopy. As shown in Figure 5A, upon STS-mediated caspase-3 activation, the overall TP fluorescence increased depending on the incubation time and all the cells showed strong TP fluorescence signals after a 2 h incubation with STS. Furthermore, the cells undergoing apoptosis showed shrinkage, budding, and apoptotic body formation with maximum TP fluorescence signals. To validate whether the fluorescence signal was specific to caspase-3 activation, we further performed experiment using DEASPI/βCDP@Ad-DEVD-BHQ2 nanoconjugate with STS and Z-DEVD-FMK. As shown in Figure 5A,f, with the nanosensing conjugate-incubated HeLa cells treated using STS for 3 h together with Z-DEVD-FMK, we did not obtain obvious fluorescence contrast, which confirmed the specificity of our live-cell imaging strategy to caspase-3 activation. These results clearly demonstrate that the fluorescence activation in apoptotic cells was specific to caspase-3 activation.

To further verify the internalization of DEASPI/βCDP@Ad-DEVD-BHQ2 nanosensing conjugates in apoptotic HeLa cells, *Z*-scanning confocal imaging was performed (Figure S7, Supporting Information). It was clear that bright fluorescence was present throughout the whole cells, which suggested efficient delivery of the nanosensing conjugate in the cytosol. This revealed that the nanosensing conjugate afforded a robust intracellular protease sensor for high-contrast TPE imaging of caspase-3 activation in live cells.

In addition to the live cells, to further show the utility of the DEASPI/βCDP@Ad-DEVD-BHQ2 nanosensing conjugate for imaging apoptosis in deep tissues, we monitored apoptosis in a 1.0 mm-thick living cervical tumor tissue slice pretreated with or without doxorubicin by using TP confocal microscope for fluorescence emission detection after the nanoconjugate incubation. The TP confocal fluorescence images showed that the DEASPI/βCDP@Ad-DEVD-BHQ2 nanoconjugate provided high TPE fluorescence emission signal for the tumor tissue slice treated with doxorubicin, indicating enabled clear visualization of apoptosis in cervical tumor tissue (Figure 5C, a). More importantly, the *Z*-scanning confocal imaging shows that clear TP fluorescence emission can still be detected until the 360 μm of penetration depth (Figure 5D), which is much deeper than that obtained from single-photon imaging (Figure S8, Supporting Information). Then, the 3D reconstitution of confocal *XYZ* scanning micrographs is obtained from 50 confocal *Z*-scan two-photon imaging sections (Figure 5C, b). In contrast, the TPE fluorescence emission signal from the

dx.doi.org/10.1021/ac503546r | *Anal. Chem.* 2014, 86, 11440−11450

nondoxorubicin-treated tumor tissue slice was substantially weaker (Figure 5B), and no significant TPE or OPE fluorescence emission can be observed in the various penetration depth (Figure S9, Supporting Information). Overall, our data presented show that the prepared nanoconjugate can be used for high-contrast TPE imaging of caspase-3 activation in apoptotic and deep tumor tissues.

CONCLUSION

In summary, we have successfully developed a TPA nanomicelle-based two-photon fluorescent nanoprobe for enzymatic activities assay in living cells and tissues with high sensitivity and selectivity. This βCDP nanomicelle-based TPA fluorescent nanoconjugate exhibits desirable two-photon-sensitized fluorescence properties, high cell-permeability, high stability and excellent biocompatibility. Compared with the nowadays prevailing strategy of OPE-based fluorescent biosensor construction, introduction of the TPE effectively eliminates the self-absorption and autofluorescence of the biological molecules in biological matrixes, reduces the photodamage resulted from the high-energy excitation, and enhances the penetration depth and spatial resolution, thus substantially improves the performance of the fluorescent sensors in complex biological conditions. In vitro assays revealed that the DEASPI/βCDP nanomicelle-based TPA fluorescent nanoconjugate provided a robust, sensitive and selective sensor for quantitative detection of caspase-3 even if under complex biological conditions. TP confocal fluorescence microscopy experiments with HeLa cells and tissues suggested that the βCDP nanomicelle-based conjugate was efficiently delivered into live cells and acted as a "signal-on" fluorescent sensor for specific, high-contrast imaging of target biomolecules. To the best of our knowledge, it is the first time that a TPA nanomicelle-based two-photon fluorescent nanoprobe has been successfully used for enzymatic activities assay in living cells and tissues. Considering the unique properties of βCDP-based nanomaterials and the TPM technique, this new TPA DEASPI/βCDP nanomicelle-based strategy for developing robust biomolecules sensors is expected to hold great potential for in vitro and in vivo applications in medical research and clinical diagnostics.

ASSOCIATED CONTENT

Supporting Information

Additional information as noted in text. This material is available free of charge via the Internet at http://pubs.acs.org.

AUTHOR INFORMATION

Corresponding Authors

*J. Li. E-mail: jishanli@hnu.edu.cn. Fax: +86-731-88822587.
*R. Yang. E-mail: yangrh@pku.edu.cn.

Notes

The authors declare no competing financial interest.

ACKNOWLEDGMENTS

This work was supported by NSFC (21475036, 21135001 and 21205143) and the "973" National Key Basic Research Program (2011CB91100-0).

REFERENCES

(1) Sharma, P.; Brown, S.; Walter, G.; Santra, S.; Moudgil, B. *Adv. Colloid Interface Sci.* **2006**, *123*, 471−485.
(2) Chen, Z.; Chen, H.; Hu, H.; Yu, M.; Li, F.; Zhang, Q.; Zhou, Z.; Yi, T.; Huang, C. *J. Am. Chem. Soc.* **2008**, *130*, 3023−3029.
(3) (a) Amy, R. L.; Storb, R. *Science* **1965**, *150*, 756−758. (b) Denk, W.; Strickler, J. H.; Webb, W. W. *Science* **1990**, *248*, 73−76. (c) Helmchen, F.; Denk, W. *Nat. Methods* **2005**, *2*, 932−940. (d) Kawata, S.; Kawata, Y. *Chem. Rev.* **2000**, *100*, 1777−1788.
(4) (a) Bae, S. K.; Heo, C. H.; Choi, D. J.; Sen, D.; Joe, E. H.; Cho, B. R.; Kim, H. M. *J. Am. Chem. Soc.* **2013**, *135*, 9915−9923. (b) Kang, D. E.; Lim, C. S.; Kim, J. Y.; Kim, E. S.; Chun, H. J.; Cho, B. R. *Anal. Chem.* **2014**, *86*, 5353−5359.
(5) (a) Liu, L. Z.; Dong, X. H.; Lian, W. L.; Peng, X. N.; Liu, Z. H.; He, Z. K.; Wang, Q. Q. *Anal. Chem.* **2010**, *82*, 1381−1388. (b) Dong, X. H.; Heo, C. H.; Chen, S. Y.; Kim, H. M.; Liu, Z. H. *Anal. Chem.* **2014**, *86*, 308−311. (c) Zhou, L. Y.; Zhang, X. B.; Wang, Q. Q.; Lv, Y. F.; Mao, G. J.; Luo, A. L.; Wu, Y. X.; Wu, Y.; Zhang, J.; Tan, W. H. *J. Am. Chem. Soc.* **2014**, *136*, 9838−9841.
(6) (a) Ding, D.; Goh, C. C.; Feng, G. X.; Zhao, Z. J.; Liu, J.; Liu, R. R.; Tomczak, N.; Geng, J. L.; Tang, B. Z.; Ng, L. G.; Liu, B. *Adv. Mater.* **2013**, *25*, 6083−6088. (b) Son, J. H.; Lim, C. S.; Han, J. H.; Danish, I. A.; Kim, H. M.; Cho, B. R. *J. Org. Chem.* **2011**, *76*, 8113−8116.
(7) (a) Wang, X. H.; Morales, A. R.; Urakami, T.; Zhang, L. F.; Bondar, M. V.; Komatsu, M.; Belfield, K. D. *Bioconjugate Chem.* **2011**, *22*, 1438−1450. (b) Wang, X. H.; Nguyen, D. M.; Yanez, C. O.; Rodriguez, L.; Ahn, H. Y.; Bondar, M. V.; Belfield, K. D. *J. Am. Chem. Soc.* **2010**, *132*, 12237−12239.
(8) (a) Baggaley, E.; Cao, D. K.; Sykes, D.; Botchway, S. W.; Weinstein, J. A.; Ward, M. D. *Chem.—Eur. J.* **2014**, *20*, 8898−8903. (b) Shen, X. Q.; Li, L.; Chan, A. C. M.; Gao, N. Y.; Yao, S. Q.; Xu, Q. H. *Adv. Optical Mater.* **2013**, *1*, 92−99. (c) Wang, G.; Pu, K. Y.; Zhang, X. H.; Li, K.; Wang, L.; Cai, L. P.; Ding, D.; Lai, Y. H.; Liu, B. *Chem. Mater.* **2011**, *23*, 4428−4434. (d) Geng, J. L.; Goh, C. C.; Tomczak, N.; Liu, J.; Liu, R. R.; Ma, L.; Ng, L. G.; Gurzadyan, G. G.; Liu, B. *Chem. Mater.* **2014**, *26*, 1874−1880.
(9) Biwersi, J.; Verkman, A. S. *Biochemistry* **1991**, *30*, 7879−7883.
(10) Wu, C. F.; Chiu, D. T. *Angew. Chem., Int. Ed.* **2013**, *52*, 3086−3109.
(11) (a) He, X. X.; Wang, K. M.; Tan, W. H.; Liu, B.; Lin, X.; He, C. M.; Li, D.; Huang, S. S.; Li, J. *J. Am. Chem. Soc.* **2003**, *125*, 7168−7169. (b) Kneuer, C.; Sameti, M.; Bakowsky, U.; Schiestel, T.; Schirra, H.; Schmidt, H.; Lehr, C. M. *Bioconjugate Chem.* **2000**, *11*, 926−932. (c) Roy, I.; Ohulchanskyy, T. Y.; Bharali, D. J.; Pudavar, H.; Mistretta, R. A.; Kaur, N.; Prasad, P. N. *Proc. Natl. Acad. Sci. U. S. A.* **2005**, *102*, 279−284.
(12) (a) Criscione, J. M.; Le, B. L.; Stern, E.; Brennan, M.; Rahner, C.; Papademetris, X.; Fahmy, T. M. *Biomaterial.* **2009**, *30*, 3946−3955. (b) Qu, T. H.; Wang, A. R.; Yuan, J. F.; Shi, J. H.; Gao, Q. Y. *Colloids Surf., B* **2009**, *72*, 94−100.
(13) Kim, T. W.; Chung, P. W.; Slowing, I. I.; Tsunoda, M.; Yeung, E. S.; Lin, V. S. Y. *Nano Lett.* **2008**, *8*, 3724−3727.
(14) (a) Winzer, T.; Knorr, A.; Malic, E. *Nano Lett.* **2010**, *10*, 4839−4843. (b) Jana, A.; Devi, K. S. P.; Maiti, T. K.; Pradeep Singh, N. D. *J. Am. Chem. Soc.* **2012**, *134*, 7656−7659.
(15) Guardado-Alvarez, T. M.; Devi, L. S.; Russell, M. M.; Schwartz, B. J.; Zink, J. I. *J. Am. Chem. Soc.* **2013**, *135*, 14000−14003.
(16) Yan, H. H.; Wang, L.; Wang, J. Y.; Weng, X. F.; Lei, H.; Wang, X. X.; Jiang, L.; Zhu, J. H.; Lu, W. Y.; Wei, X. B.; Li, C. *ACS Nano* **2012**, *6*, 410−420.
(17) (a) Larson, D. R.; Zipfel, W. R.; Williams, R. M.; Clark, S. W.; Bruchez, M. P.; Wise, F. W.; Webb, W. W. *Science* **2003**, *300*, 1434−1436. (b) Gao, X.; Cui, Y.; Levenson, R. M.; Chung, L. W. K.; Nie, S. *Nat. Biotechnol.* **2004**, *22*, 969−976.
(18) (a) Wang, J. Z.; Lin, M.; Yan, Y. L.; Wang, Z.; Ho, P. C.; Loh, K. P. *J. Am. Chem. Soc.* **2009**, *131*, 11300−11301. (b) Jauffred, L.; Oddershede, L. B. *Nano Lett.* **2010**, *10*, 1927−1930.
(19) (a) Ramakrishna, G.; Varnavski, O.; Kim, J.; Lee, D.; Goodson, T. *J. Am. Chem. Soc.* **2008**, *130*, 5032−5033. (b) Patel, S. A.; Richards, C. I.; Hsiang, J. C.; Dickson, R. M. *J. Am. Chem. Soc.* **2008**, *130*, 11602−11603.

(20) (a) Li, J. L.; Bao, H. C.; Hou, X. L.; Sun, L.; Wang, X. G.; Gu, M. *Angew. Chem., Int. Ed.* **2012**, *51*, 1830−1834. (b) Zhu, A. W.; Qu, Q.; Shao, X. L.; Kong, B.; Tian, Y. *Angew. Chem., Int. Ed.* **2012**, *51*, 7185−7189.
(21) (a) Li, J. L.; Bao, H. C.; Hou, X. L.; Sun, L.; Wang, X. G.; Gu, M. *Angew. Chem., Int. Ed.* **2012**, *51*, 1830−1834. (b) Liu, Q.; Guo, B. D.; Rao, Z. Y.; Zhang, B. H.; Gong, J. R. *Nano Lett.* **2013**, *13*, 2436−2441.
(22) Li, J. L. Y.; Goh, C. C.; Keeble, J. L.; Qin, J. S.; Roediger, B.; Jain, R.; Wang, Y.; Chew, W. K.; Weninger, W.; Ng, L. G. *Nat. Protoc.* **2012**, *7*, 221−234.
(23) (a) Luo, P. G.; Sahu, S.; Yang, S.-T.; Sonkar, S. K.; Wang, J. P.; Wang, H. F.; LeCroy, G. E.; Cao, L.; Sun, Y. P. *J. Mater. Chem. B* **2013**, *1*, 2116−2127. (b) Li, L. L.; Wu, G. H.; Yang, G. H.; Peng, J.; Zhao, J. W.; Zhu, J. J. *Nanoscale* **2013**, *5*, 4015−4039.
(24) Liu, R.; Zhang, Y.; Feng, P. Y. *J. Am. Chem. Soc.* **2009**, *131*, 15128−15129.
(25) (a) Kulkarni, A.; Deng, W.; Hyun, S.; Thompson, D. H. *Bioconjugate Chem.* **2012**, *23*, 933−940. (b) Liu, Y.; Yu, L.; Chen, Y.; Zhao, Y. L.; Yang, H. *J. Am. Chem. Soc.* **2007**, *129*, 10656−10657.
(26) Davis, M. E.; Brewster, M. E. *Nature Rev.* **2004**, *3*, 1023−1035.
(27) Yan, H. J.; He, L. L.; Ma, C.; Li, J. S.; Yang, J. F.; Yang, R. H.; Tan, W. H. *Chem. Commun.* **2014**, *50*, 8398−8401.
(28) (a) Budihardjo, I.; Oliver, H.; Lutter, M.; Luo, X.; Wang, X. D. *Annu. Rev. Cell Dev. Biol.* **1999**, *15*, 269−290. (b) Green, D. R. *Cell* **1998**, *94*, 695−698. (c) Thornberry, N. A.; Lazebnik, Y. *Science.* **1998**, *281*, 1312−1316.
(29) Lee, S.; Choi, K. Y.; Chung, H.; Ryu, J. H.; Lee, A.; Koo, H.; Youn, I. C.; Park, J. H.; Kim, I. S.; Kim, S. Y.; Chen, X. Y.; Jeong, S. Y.; Kwon, I. C.; Kim, K.; Choi, K. *Bioconjugate Chem.* **2011**, *22*, 125−131.
(30) (a) Wang, H. B.; Zhang, Q.; Chu, X.; Chen, T. T.; Ge, J.; Yu, R. Q. *Angew. Chem., Int. Ed.* **2011**, *50*, 7065−7069. (b) Boeneman, K.; Mei, B. C.; Dennis, A. M.; Bao, G.; Deschamps, J. R.; Mattoussi, H.; Medintz, I. L. *J. Am. Chem. Soc.* **2009**, *131*, 3828−3829.
(31) (a) Shi, H. B.; Kwok, R. T. K.; Liu, J. Z.; Xing, B. G.; Tang, B. Z.; Liu, B. *J. Am. Chem. Soc.* **2012**, *134*, 17972−17981. (b) Yuan, Y. Y.; Kwok, R.T. K.; Tang, B. Z.; Liu, B. *J. Am. Chem. Soc.* **2014**, *136*, 2546−2554.
(32) Pop, C.; Chen, Y. R.; Smith, B.; Bose, K.; Bobay, B.; Tripathy, A.; Franzen, S.; Clark, A. C. *Biochemistry* **2001**, *40*, 14224−14235.
(33) (a) Kim, S.; Ohulchanskyy, T. Y.; Pudavar, H. E.; Pandey, R. K.; Prasad, P. N. *J. Am. Chem. Soc.* **2007**, *129*, 2669−2675. (b) Sreejith, S.; Ma, X.; Zhao, Y. L. *J. Am. Chem. Soc.* **2012**, *134*, 17346−17349. (c) Jin, Y. H.; Lohstreter, S.; Pierce, D. T.; Parisien, J.; Wu, M.; Hall, C.; Zhao, X. J. *Chem. Mater.* **2008**, *20*, 4411−4419. (d) Xie, J.; Liu, G.; Eden, H. S.; Ai, H.; Chen, X. Y. *Acc. Chem. Res.* **2011**, *44*, 883−892.
(34) Verma, A.; Stellacci, F. *Small* **2010**, *6*, 12−21.
(35) Marsh, M. H.; McMahon, T. *Science* **1999**, *285*, 215−220.
(36) Mukherjee, S.; Ghosh, R. N.; Maxfield, F. R. *Physiol. Rev.* **1997**, *77*, 759−803.
(37) (a) Mosmann, T. *J. Immunol. Methods* **1983**, *65*, 55−63. (b) Liu, Y. B.; Peterson, D. A.; Kimura, H.; Schubert, D. *J. Neurochem.* **1997**, *69*, 581−593.
(38) Sun, I. C.; Lee, S.; Koo, H.; Kwon, I. C.; Choi, K.; Ahn, C. H.; Kim, K. *Bioconjugate Chem.* **2010**, *21*, 1939−1942.
(39) Fu, C. C.; Lee, H. S.; Chen, K.; Lim, T. S.; Wu, H. Y.; lin, P. K.; Wei, P. K.; Tsao, P. H.; Chang, H. C.; Fann, W. S. *Proc. Natl. Acad. Sci. U. S. A.* **2007**, *104*, 727−732.
(40) Lin, S. Y.; Chen, N. T.; Sun, S. P.; Chang, J. C.; Wang, Y. C.; Yang, C. S.; Lo, L. W. *J. Am. Chem. Soc.* **2010**, *132*, 8309−8315.